Ultra-fast laser pulses as a probe of electron dynamics: A next generation QTAIM perspective

SUPPLEMENTARY MATERIALS

Chirality and Ultra-Fast Laser Irradiation

Huan He[1], Xiao Peng Mi[1], Xinjie Zhou[1], Genwei Hong[1], Tianlv Xu[1], Herbert Früchtl[2], Tanja van Mourik[2], Martin, J. Paterson[3], Steven R. Kirk[*1] and Samantha Jenkins[*1]

[1]Key Laboratory of Chemical Biology and Traditional Chinese Medicine Research and Key Laboratory of Resource National and Local Joint Engineering Laboratory for New Petro-chemical Materials and Fine Utilization of Resources, College of Chemistry and Chemical Engineering, Hunan Normal University, Changsha, Hunan 410081, China
[2]EaStCHEM School of Chemistry, University of Saint Andrews, North Haugh, St Andrews, Fife KY16 9ST, Scotland, United Kingdom.
[3]Institute of Chemical Sciences, School of Engineering and Physical Sciences, Heriot-Watt University, Edinburgh, EH14 4AS, UK

email: steven.kirk@cantab.net
email: samanthajsuman@gmail.com

1. Supplementary Materials S1. NG-QTAIM theoretical background and procedure to generate the Hessian of $\rho(\mathbf{r})$ eigenvector-following trajectories $\mathbb{T}_{\mathbf{F}}(s)$.

2. Supplementary Materials S2. Specification of the electric field, generation of the gridded total electronic charge density distribution $\boldsymbol{\rho}(\mathbf{r})$ and tabulated Excitation frequencies ω.

3. Supplementary Materials S3. Populations of the multi-reference superposition states for a selection of electric **E**-field values.

4. Supplementary Materials S4. Maximum Hessian of $\rho(\mathbf{r})$ eigenvector-following trajectory projections $\mathbb{T}_{\mathbf{F}max}(s)$ tables for the C1-C2 *BCP*s.

1. Supplementary Materials S1. NG-QTAIM theoretical background and procedure to generate the Hessian of $\rho(\mathbf{r})$ eigenvector-following trajectories $\mathbb{T}_F(s)$.

1(a) *QTAIM bond critical point (BCP) properties; ellipticity ε:*

The four types of QTAIM critical points are labeled using the notation (R, ω) where R is the rank of the Hessian matrix, i.e., the number of distinct non-zero eigenvalues and ω is the signature (the algebraic sum of the signs of the eigenvalues); the (3, -3) [nuclear critical point (*NCP*), a local maximum], (3, -1) and (3, 1) [saddle points, referred to as bond critical points (*BCP*) and ring critical points (*RCP*), respectively] and (3, 3) [the cage critical points (*CCP*)]. In the limit that the forces on the nuclei are zero, an atomic interaction line[1] the line passing through a *BCP* and terminating on two nuclear attractors along which the charge density $\rho(\mathbf{r})$ is locally maximal with respect to nearby lines, becomes a bond-path[2]. The full set of critical points with the bond-paths of a molecule or cluster is referred to as the molecular graph.

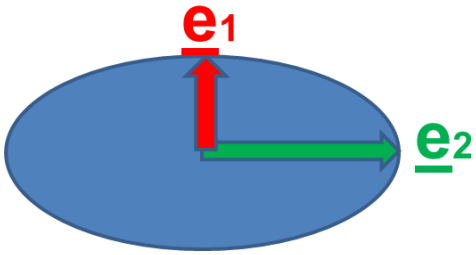

Scheme S1. The cross section through a bond at the bond critical point (*BCP*). The λ_1 and λ_2 eigenvalues with associated eigenvectors $\underline{\mathbf{e}}_1$ and $\underline{\mathbf{e}}_2$ respectively, define the axes of the ellipse and indicate the magnitudes of the least and greatest extents of the distribution of $\rho(\mathbf{r})$.

The ellipticity, ε, defined as $\varepsilon = |\lambda_1|/|\lambda_2| - 1$, quantifies the relative accumulation of the electronic charge density $\rho(\mathbf{r_b})$ distribution in the two directions $\underline{\mathbf{e}}_1$ and $\underline{\mathbf{e}}_2$ that are perpendicular to the bond-path at a Bond Critical Point (*BCP*) with position $\mathbf{r_b}$. For ellipticity $\varepsilon > 0$, the shortest and longest axes of the elliptical distribution of $\rho(\mathbf{r_b})$ are associated with the λ_1 and λ_2 eigenvalues, respectively. From the electron-preceding perspective a change in the electronic charge density distribution that defines a chemical bond causes in a change in atomic positions[3]. Bone and Bader later proposed that the direction of motion of the atoms that results from a slightly perturbed structure coincides with the direction of motion of the electrons[4]; this was later confirmed[5], [6].

1(b) *QTAIM bond-path properties; bond-path length (BPL)* **:**

The bond-path length (BPL) is defined as the length of the path traced out by the $\underline{\mathbf{e}}_3$ eigenvector of the Hessian of the total charge density $\rho(\mathbf{r})$, passing through the *BCP*, along which $\rho(\mathbf{r})$ is locally maximal with respect to any neighboring paths. The bond-path curvature separating two bonded nuclei is defined as the dimensionless ratio

(BPL - GBL)/GBL, where the BPL is defined to be the bond-path length associated and GBL is the inter-nuclear separation. The BPL often exceeds the GBL particularly in strained bonding environments[5]. Earlier, one of the current authors hypothesized that a bond-path may possess 1-D, 2-D or a 3-D morphology[7], with 2-D or a 3-D bond-paths associated with a *BCP* with ellipticity $\varepsilon > 0$, being due to the differing degrees of charge density accumulation, of the λ_2 and λ_1 eigenvalues respectively. Bond-paths possessing zero and non-zero values of the bond-path curvature defined by equation **(2)** can be considered to possess 1-D and 2-D topologies respectively. We start by choosing the length traced out in 3-D by the path swept by the tips of the scaled $\underline{\mathbf{e}}_2$ eigenvectors of the λ_2 eigenvalue, the scaling factor being chosen as the ellipticity ε, see **Scheme S1**.

Full Symmetry-breaking for Iso-Energetic Phenomena: Derivation and numerical procedure of the second-generation eigenvector-space trajectory $\mathbb{T}_i(\boldsymbol{s})$

1(a) *The Second-Generation eigenvector-space trajectories*: $\mathbb{T}_i(\boldsymbol{s})$; $i = \{\rho\}$ *for Stereochemistry:*

The maximum eigenvector projections $\mathbb{T}(\boldsymbol{s})_{\mathbf{max}} = \{t_{1\mathbf{max}}, t_{2\mathbf{max}}, t_{3\mathbf{max}}\}$ are used to define the dimensions of a 'bounding box' around each $\mathbb{T}(\boldsymbol{s})$ and are used to calculate the chirality $\mathbb{C}$, bond-flexing $\mathbb{F}$ and bond-axiality $\mathbb{B}$. The subscript '$_{\mathbf{max}}$' corresponds to the difference between the minimum and maximum value of the projection of the *BCP* shift **dr** onto $\underline{\mathbf{e}}_1$, $\underline{\mathbf{e}}_2$ or $\underline{\mathbf{e}}_3$ along the entire $\mathbb{T}(\boldsymbol{s})$. Note: the $\mathbf{e}_2$ corresponds to the direction in which the electrons at the *BCP* are subject to the most compressive forces[8], therefore $\mathbf{e}_2$ corresponds to the most *facile direction* for displacement of the *BCP* electrons when the *BCP* is torsioned. Conversely the $\mathbf{e}_1$ and $\mathbf{e}_3$ correspond to the directions associated with the least compressive forces and the tensile forces on the *BCP* electrons respectively.

The chirality $\mathbb{C}$ is generated from the $\boldsymbol{t}_2 = \underline{\mathbf{e}}_2 \cdot \mathbf{dr}$ (bond-twist) *BCP* shift in the plane perpendicular to $\underline{\mathbf{e}}_3$ (the bond-path) and is defined by the difference in the maximum $\mathbb{T}(\boldsymbol{s})$ projections (the dot product of the eigenvector $\underline{\mathbf{e}}_2$ eigenvector and the *BCP* shift **dr**) of the $\mathbb{T}(\boldsymbol{s})$ values between the CCW and CW torsions:

$$\mathbb{C} = [(\underline{\mathbf{e}}_2 \cdot \mathbf{dr})_{\mathbf{max}}]_{\mathrm{CCW}} - [(\underline{\mathbf{e}}_2 \cdot \mathbf{dr})_{\mathbf{max}}]_{\mathrm{CW}} \qquad \textbf{(S1.1)}$$

The bond-flexing $\mathbb{F}$ is generated from $\boldsymbol{t}_1 = \underline{\mathbf{e}}_1 \cdot \mathbf{dr}$ where $\underline{\mathbf{e}}_1$ corresponds to the least facile Hessian of $\rho(\mathbf{r})$ eigenvector:

$$\mathbb{F} = [(\underline{\mathbf{e}}_1 \cdot \mathbf{dr})_{\mathbf{max}}]_{\mathrm{CCW}} - [(\underline{\mathbf{e}}_1 \cdot \mathbf{dr})_{\mathbf{max}}]_{\mathrm{CW}} \qquad \textbf{(S1.2)}$$

The bond-axiality $\mathbb{A}$ is generated from the axial *BCP* sliding $t_3 = \underline{e}_3 \cdot \mathbf{dr}$[9], where the *BCP* sliding is the shift of the *BCP* position along the containing bond-path:

$$\mathbb{A} = [(\underline{e}_3 \cdot \mathbf{dr})_{max}]_{CCW} - [(\underline{e}_3 \cdot \mathbf{dr})_{max}]_{CW} \qquad \textbf{(S1.3)}$$

and quantifies the resultant extent of *axial* displacement of the *BCP* in response to the bond torsion (CCW vs. CW), i.e. the sliding of the *BCP* along the bond-path[9].

The sign (+) or (-) of each of the chirality $\mathbb{C}$, bond-flexing $\mathbb{F}$ and bond-axiality $\mathbb{A}$ from equations **(S1.1)-(S1.3)** respectively determines the presence of **S** character for $\mathbb{C} > 0$, $\mathbb{F} > 0$ or $\mathbb{A} > 0$ and **R** character for $\mathbb{C} < 0$, $\mathbb{F} < 0$ or $\mathbb{A} < 0$. The complete set {bond-flexing $\mathbb{F}$, chirality $\mathbb{C}$, bond axiality $\mathbb{A}$} is referred to as the *distortion* set.

A helical response of the $\rho(\mathbf{r_b})$ both non-axial, perpendicular to the bond-path and axial (parallel to the bond-path) displacements of the torsional C1-C2 *BCP* may be found, see the helical shaped $\mathbb{T}(s)$. The circumstances that lead to helical or linear trajectories $\mathbb{T}(s)$ are not limited to chiral molecules, but also apply to formally achiral molecules that have the capacity to become chiral when subject to suitable substitution. The chirality-helicity function $\mathbb{C}_{helicity}$ is the arithmetic product of the circular ($\mathbb{C}$) and the magnitude of the axial ($\mathbb{A}$) displacement and consequently quantifies the resultant displacement of the torsional *BCP*:

$$\mathbb{C}_{helicity} = (\text{chirality } \mathbb{C}) \times (|\text{axiality } \mathbb{A}|) = \mathbb{C}|\mathbb{A}| \qquad \textbf{(S1.4)}$$

2(b) *Numerical Considerations for Calculation of the Second-Generation Eigenvector-Space Trajectory* $\mathbb{T}_i(s)$

Central to the concept of the second-generation eigenvector-space trajectory $\mathbb{T}_i(s)$ is the concept of a monotonically increasing sequence parameter s, which may take the form of an increasing integer sequence (0, 1, 2, 3,...) in applications where a set of discrete numbered steps are involved, or a continuous real number. The 3-D eigenvector trajectory $\mathbb{T}_i(s)$ is then defined as an ordered set of points, whose sequence is described by the parameter s. In this application, we used an integer step number for s. We first choose to associate $s = 0$ with a specific reference molecular graph, in this case, the energy minimum structure. For a specific *BCP*, the coordinates associated with each of the points are calculated by evaluating the components of the shift vector **dr**

= $\mathbf{r}_b(s) - \mathbf{r}_b(s\text{-}1)$ where $\mathbf{r}_b$ indicates the location of the *BCP*, from the previous step to the current step in the reference coordinate frame defined by the eigenvectors $\underline{\mathbf{e}}_1$, $\underline{\mathbf{e}}_2$, $\underline{\mathbf{e}}_3$.

Note: for displaying the eigenvector trajectories $\mathbb{T}_i(s)$, large steps that can occur at the beginning or end of a $\mathbb{T}_i(s)$ may swamp the appearance of the $\mathbb{T}_i(s)$. To solve this we temporarily filter these steps before including them back in to correctly calculate the $\mathbb{U}_\sigma$-space eigenvector trajectory $\mathbb{T}_i(s)$.

The calculation of the $\mathbb{T}_i(s)$ is made easier if the code which produces the list of structures corresponding to points along each step of the torsion (CW) and counterclockwise CCW generates these structures at regularly-spaced points. The consequence of this desirable characteristic is that there are few or no large changes or 'spikes' in the magnitude of the *BCP* shift vector **dr** i.e. $\Delta\mathbf{dr}$, between path step s and $s + 1$. Such anomalies occur because some path-following algorithms may employ occasional small predictor-corrector steps that are at least an order of magnitude smaller than standard steps. In this analysis it is observed that such intermittent relatively small steps in turn cause very small shifts **dr** to be interspersed between longer runs of larger changes, causing 'spike' noise in the otherwise smooth trajectories $\mathbb{T}_i(s)$. Such 'spikes', which usually only consist of a single spurious point deviating from the locally smooth eigenvector trajectory, can make potentially large spurious contributions to the eigenvector trajectory $\mathbb{T}_i(s)$ and may be safely filtered. A combination of criteria are recommended for automated rejection of inclusion of a specific point into the trajectories $\mathbb{T}_i(s)$:

1. If the magnitude of the **dr** associated with any current $\mathbb{T}_i(s)$ point is less than 50% of the average of the corresponding **dr** values associated with the immediately preceding point and the immediately following point, the current point is filtered out as a ‘spike’.
2. Abrupt changes in direction in the $\mathbb{T}_i(s)$, e.g. turning by more than 60^0 from one $\mathbb{T}_i(s)$ step to the next cause the current point to be labelled as a ‘spike’.

These two rules taken together are referred to as the ‘turn’ filter. These rules can be repeatedly applied across multiple ‘passes’ through the eigenvector trajectory data as necessary.

It has been observed that the magnitudes of the steps **dr** naturally tend to slowly decrease toward the end of paths, corresponding to a slowed approach to an end minimum, and the corresponding part of the $\mathbb{T}_i(s)$ turns toward the $\mathbb{U}_i$-space origin. A combination of the criteria mentioned above may be deployed to retain these parts of the $\mathbb{T}_i(s)$.

An alternative Kolmogorov-Zurbenko[10] data ‘smoothing’ filter may also be applied.

References

[1] R. F. W. Bader, *J. Phys. Chem. A*, **1998**, DOI:10.1021/jp981794v.

[2] R. F. W. Bader, *J. Phys. Chem. A*, **2009**, DOI:10.1021/jp906341r.
[3] H. Nakatsuji, *J. Am. Chem. Soc.*, **1974**, DOI:10.1021/ja00808a004.
[4] R. G. A. Bone, R. F. W. Bader, *J. Phys. Chem.*, **1996**, DOI:10.1021/jp953512m.
[5] S. Jenkins, M. I. Heggie, *J. Phys. Condens. Matter*, **2000**, DOI:10.1088/0953-8984/12/49/3.
[6] P. W. Ayers, S. Jenkins, *J. Chem. Phys.*, **2009**, DOI:10.1063/1.3098140.
[7] S. Jenkins, I. Morrison, *Chem. Phys. Lett.*, **2000**, DOI:10.1016/S0009-2614(99)01306-8.
[8] P. Szarek, Y. Sueda, A. Tachibana, *J. Chem. Phys.*, **2008**, DOI:10.1063/1.2973634.
[9] T. Tian, T. Xu, S. R. Kirk, I. T. Rongde, Y. B. Tan, S. Manzhos, Y. Shigeta, S. Jenkins, *Phys. Chem. Chem. Phys.*, **2020**, DOI:10.1039/C9CP05879F.
[10] W. Yang, I. Zurbenko, *Wiley Interdiscip. Rev. Comput. Stat.*, **2010**, DOI:10.1002/wics.71.

2. Supplementary Materials S2. Specification of the electric field, generation of the gridded total electronic charge density distribution $\boldsymbol{\rho}(\mathbf{r})$ and tabulated Excitation frequencies ω.

Specification of the electric field E:

Commencing at the start of the electron dynamics calculation t = 0 fs, a time-dependent electric field vector $\mathbf{E}(t)$ was applied in the form of a single 10 fs duration 'sine-squared'-shaped circularly-polarized laser pulse using a range of different pulse amplitudes (i.e. peak electric field magnitudes). A circularly polarized pulse was simulated in the *yz* polarization plane with electric field components [$\mathbf{E}_y(t)$, $\mathbf{E}_z(t)$], corresponding to the molecular coordinate axes defined in **Scheme 1**. The overall field vector [$\mathbf{E}_y(t)$, $\mathbf{E}_z(t)$] was computed as the arithmetic product of three terms:

1. The 'carrier' wave, commencing at time t = 0 fs with initial phase = 0, taken as the vector [$\sin(\omega t)$, $\sin(\omega t + \pi/2)$] in the ($\boldsymbol{y}$,$\boldsymbol{z}$) polarization plane, with ω being the selected laser excitation frequency.

2. The 'amplitude envelope' of a single pulse as a half-cycle 'sine-squared'-shaped function $E_{peak} \sin^2(\omega_{env} t)$, also commencing at time t = 0 fs with phase = 0, of varying peak field amplitude E_{peak} with ω_{env} selected to give a half-cycle, i.e., yielding a single pulse, time of 10 fs. After t =10fs, the field amplitude was set to zero.

3. A polarization factor of +1 or -1, applied only to the $\mathbf{E}_z(t)$ field component: this choice yielded a resultant electric field vector which turned either clockwise [CW, +1] or counterclockwise [CCW,-1] in the ($\boldsymbol{y}$,$\boldsymbol{z}$) polarization plane with increasing time t.

Details of how to obtain the gridded total electronic charge density distribution $\boldsymbol{\rho}(\mathbf{r})$:

The total electronic charge density distribution $\rho(\mathbf{r})$ was calculated from the first-order reduced density matrix (1RDM) and saved to disk storage every 4 dynamics timesteps. At each of these '1RDM-save' timesteps, a snapshot was generated from the 1RDM as a 'gridded' scalar field of total electronic charge density $\rho(\mathbf{r})$ with a regular grid spacing of 0.1 a.u. and a grid edge padding distance of 4.0 a.u. on all sides of the molecule. These grid parameters were chosen both to ensure accurate calculation of NG-QTAIM quantities and to ensure that the integrated total electronic charge density within the chosen density grid remained constant throughout the electron dynamics simulation run.

Table S2. Excitation frequencies ω for excited states from initial time dependent density functional theory (**TDDFT**) zero electric field calculations in atomic units (au).

Electronic State	Excitation frequency ω (a.u)
S_0	0.0000000
S_1	0.3173230
S_2	0.3173230
S_3	0.3433195
S_4	0.3433195
S_5	0.3473178
S_6	0.3506694
S_7	0.3506694
S_8	0.3521798
S_9	0.3531169
S_{10}	0.3729211
S_{11}	0.3787348
S_{12}	0.3787348
S_{13}	0.3822995
S_{14}	0.3822995
S_{15}	0.3828067
S_{16}	0.3849051
S_{17}	0.3861545
S_{18}	0.3861582
S_{19}	0.3999760
S_{20}	0.4037758

3. Supplementary Materials S3. Populations of the multi-reference superposition states for a selection of electric **E**-field values.

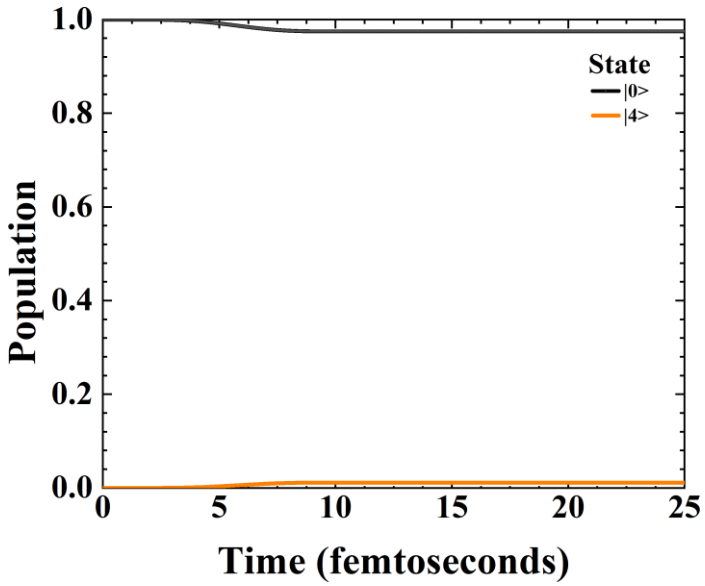

Figure S3 (a). Populations of the multi-reference superposition states for values of the electric **E**-field = 20.0 x 10^{-4} au. The variations of circular polarizations for the clockwise (**CW**) (left-panel) and counterclockwise (**CCW**) (right-panel) that are non-zero for the plane of circular polarization *yz*. Pulses are 10 fs long and the electric **E** field starts at phase = 0 at time $t = 0$ fs.

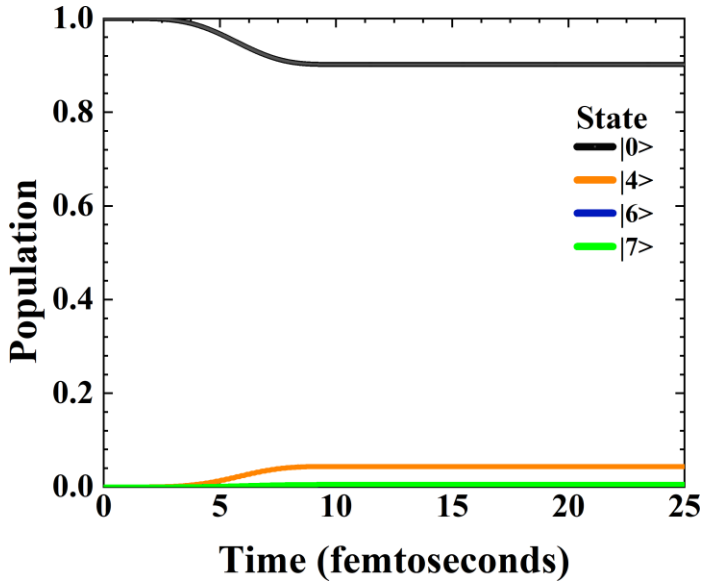

Figure S3 (b). Populations for **E** = 40.0 x 10^{-4} au. See the caption of **Figure S3 (a)** for further details.

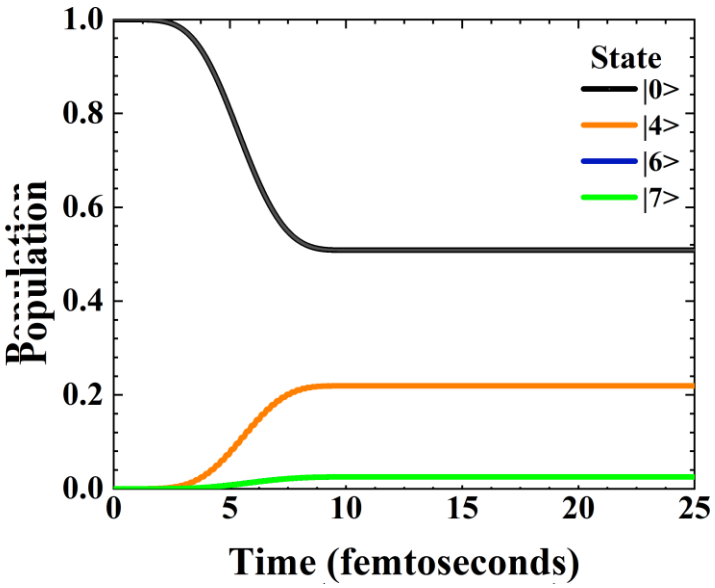

Figure S3 (c). Populations for **E** = 60.0 x 10^{-4} au. and circular polarization *yz*. See the caption of **Figure S3 (a)** for further details.

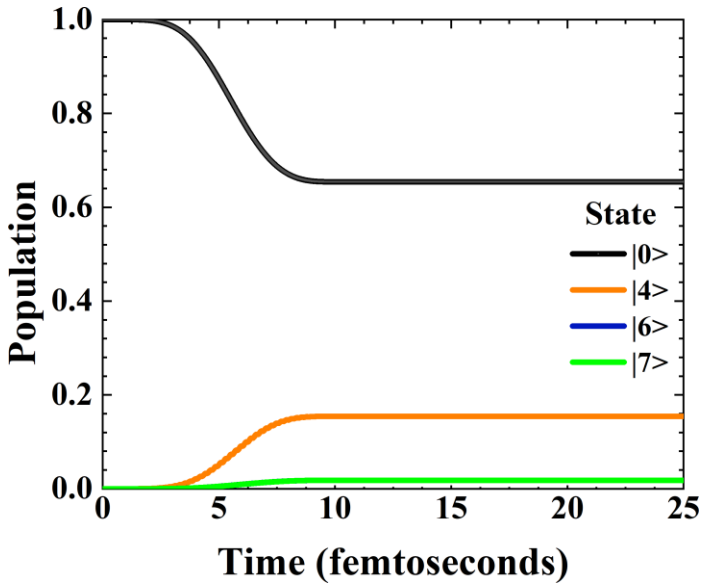

Figure S3 (d). Populations for **E** = 80.0 x 10^{-4} au. See the caption of **Figure S3 (a)** for further details.

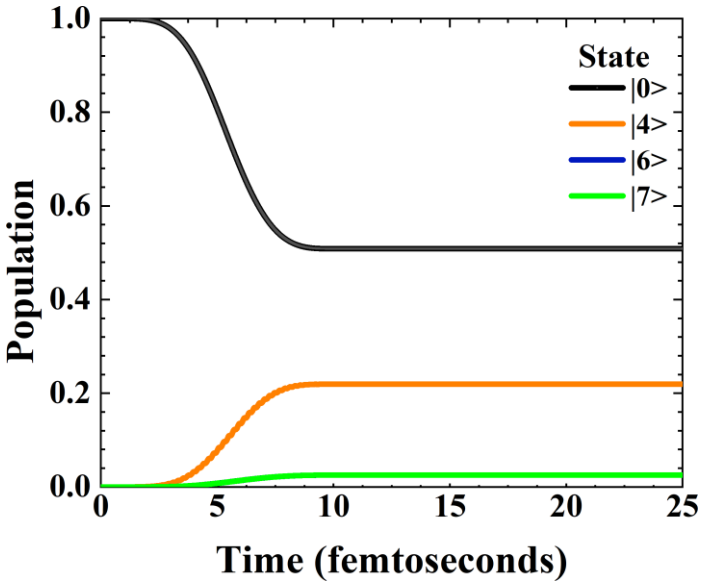

Figure S3 (e). Populations for **E** = 100.0 x 10^{-4} au. See the caption of **Figure S3 (a)** for further details.

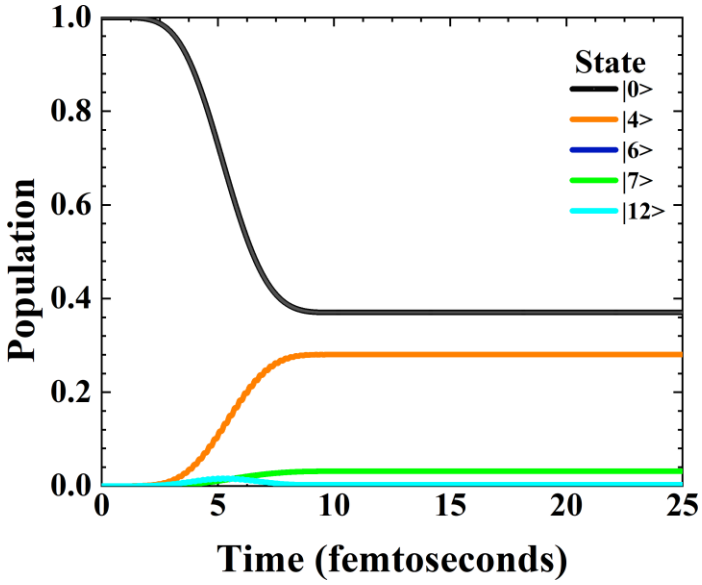

Figure S3 (f). Populations for **E** = 120.0 x 10^{-4} au. See the caption of **Figure S3 (a)** for further details.

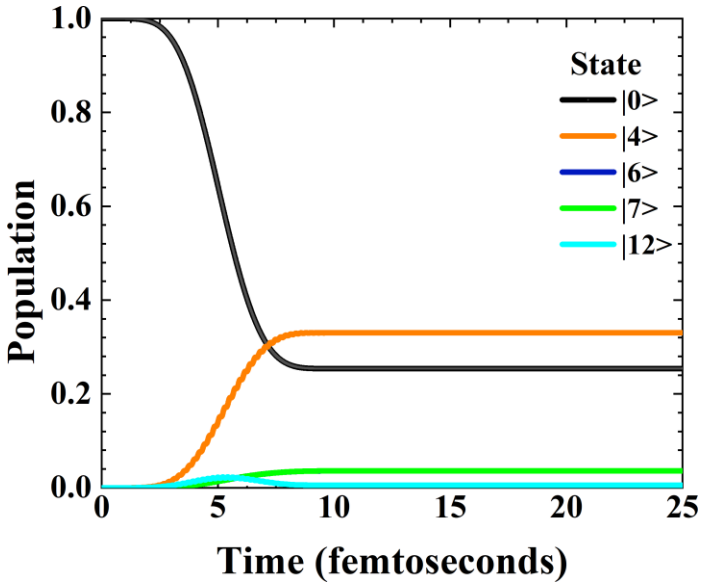

Figure S3 (g). Populations for electric field **E** = 140.0 x 10^{-4} au. See the caption of **Figure S3 (a)** for further details.

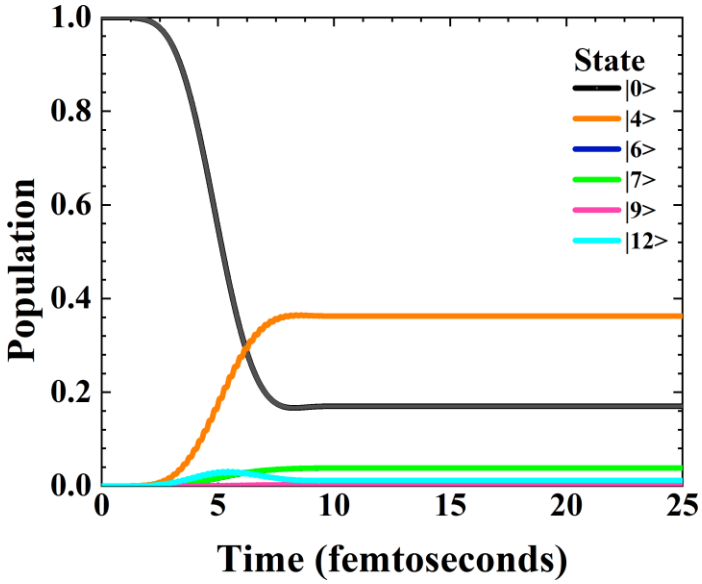

Figure S3 (h). Populations for electric field **E** = 160.0 x 10^{-4} au. See the caption of **Figure S3 (a)** for further details.

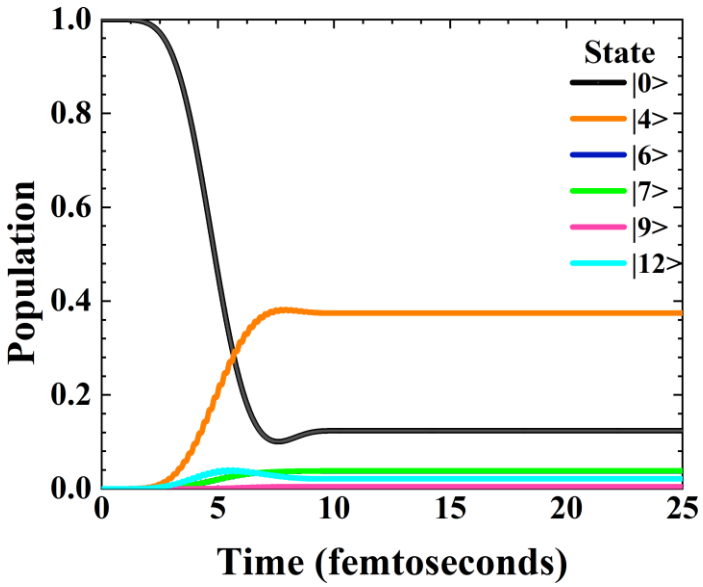

Figure S3 (i). Populations for electric field **E** = 180.0 x 10^{-4} au. See the caption of **Figure S3 (a)** for further details.

4. Supplementary Materials S4. Maximum Hessian of $\rho(\mathbf{r})$ trajectory projections $\mathbb{T}_{max}(\boldsymbol{s})$ tables for the C1-C2 *BCP*s.

Table S4. The maximum Hessian of $\rho(\mathbf{r})$ eigenvector-following trajectory projections $\mathbb{T}_{\mathbf{F}max}(s)$ = {bond-flexing$_{max}$, bond-twist$_{max}$, bond-axiality$_{max}$} where $\mathbb{F}$ = bond-flexing$_{max}$, $\mathbb{T}$ = bond-twist$_{max}$ and $\mathbb{A}$ = bond-axiality$_{max}$} of the C1-C2 *BCPs* of ethane corresponding to the right-handed **CW (R, [+1])** and left-handed **CCW (S, [-1])** with peak electric field intensity **E** in units of 10^{-4} au in the planes of polarization *yz* are provided; all entries have been multiplied by 10^3.

	$\{\mathbb{F}, \mathbb{T}, \mathbb{A}\}$	
	CW (R, [+1])	**CCW (S, [-1])**
Electric field **E**		
1.0	{0.002827, 0.002838, 0.000025}	{0.002826, 0.002839, 0.000024}
2.0	{0.005652, 0.005670, 0.000025}	{0.005649, 0.005671, 0.000025}
5.0	{0.014124, 0.014174, 0.000018}	{0.014113, 0.014171, 0.000026}
10.0	{0.028232, 0.028337, 0.000048}	{0.028213, 0.028332, 0.000048}
200.0	{0.423302, 0.436629, 0.036873}	{0.420009, 0.434054, 0.036871}